# Effects of the MYH7 R369Q Dilated Cardiomyopathy-causing Mutation on Myosin Crossbridge Kinetics and Cardiomyocyte Contractility

Agatha Carina Mae

A thesis

submitted in partial fulfillment of the

requirements for the degree of

Master of Science

University of Washington

2023

Committee:

Michael Regnier

Farid Moussavi Harami

Program Authorized to Offer Degree:

Department of Bioengineering

University of Washington

## Abstract

Effects of the MYH7 R369Q Dilated Cardiomyopathy-causing Mutation on Myosin Crossbridge Kinetics and Cardiomyocyte Contractility

Agatha Carina Mae

Chair of the Supervisory Committee:
Michael Regnier

Department of Bioengineering

The R369Q mutation in the MYH7 gene is a likely pathogenic variant of familial dilated cardiomyopathy (DCM). This mutation is located in loop 4 of β-myosin heavy chain actin-binding surface and may alter actin-myosin interaction that facilitates cardiomyocyte contraction. There are limited insights into the nature and implications of this mutation on the contractile system within a cardiomyocyte that results in hypocontractility. To better understand the biochemical and biophysical effects of R369Q mutation, this study utilized CRISPR/Cas9-edited R369Q homozygous human induced pluripotent stem cell-derived cardiomyocytes to investigate its effect on the myosin crossbridge cycle kinetics and cell contractility. The rate of ATP binding to isolated myofibrils, as measured using the stopped-flow technique, was observed to be slower for the R369Q myosin variant. As contractility is driven by transient rise of intracellular calcium, there is no significant difference between the calcium transient of healthy and R369Q mutant cardiomyocytes. These effects may contribute to the development of DCM and highlight the importance of understanding the molecular consequences of genetic mutations.

## Introduction

Cardiomyopathy is a broad term encompassing various conditions that affect the heart's structure and function, making it harder for the heart to pump blood effectively. Over time, the weakened heart muscle may become unable to meet the body's demand for blood and oxygen, leading to heart failure. Among many types of cardiomyopathies, dilated cardiomyopathy (DCM) stands out as a significant concern. DCM is a condition characterized by the enlargement and weakening of the left ventricle that serves as the heart's main pumping chamber (Fig. 1). The estimated prevalence of this disease is 1 in 250 to 400 people and it accounts for 60% of pediatric cardiomyopathies[1].

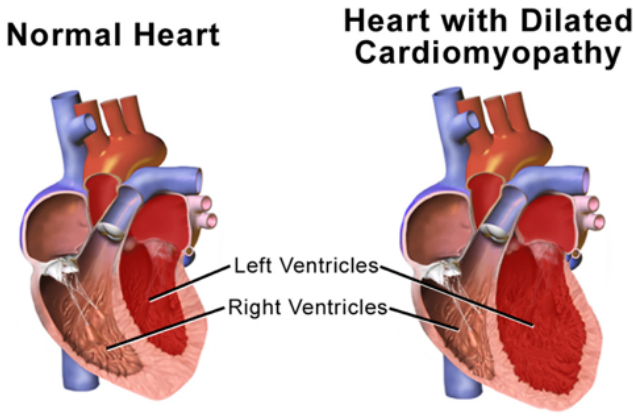


*Figure 1. DCM is characterized by the enlargement of the left ventricle*[2]

One of the key features of DCM is hypocontractility, which refers to the reduced ability of a heart muscle cell or cardiomyocyte to shorten and develop force. The weakened muscle fibers are unable to contract with the same force as a healthy heart and leads to impaired systolic function. As a result, the heart's pumping ability is compromised, and it becomes less efficient in circulating blood throughout the body. Though its commonality, DCM is a poorly understood group of disorders that result in arrythmia, heart failure, and premature death[3].

Available treatments of DCM only aim to manage symptoms, slow down the progression of the disease, and prevent complications. For mild to moderate DCM, typical treatments include a combination of lifestyle modifications and medications, such as beta-blockers and angiotensin-converting enzyme inhibitors. For patients with specific types of DCM and impaired electrical conduction in the heart, implantation of biventricular pacemaker may be recommended to coordinates the heart's contractions and improve its pumping efficiency. Heart transplantation may be considered for patients with end-stage DCM and severe heart failure. While these treatments

can enhance a patient's quality of life and life expectancy, they do not directly address the root cause of the disease. This brings about the overarching goal of this project, which is to identify specific molecular mechanism involved in the development and progression of DCM.

**Pathogenesis of DCM**

The organization of the heart encompasses multiple levels. Within the heart, there are individual cells known as cardiomyocytes. Myofibrils are found within each cardiomyocyte and considered the smallest contractile organelle in heart muscle. Each myofibril consists of repeating sarcomeres, with an individual sarcomere being referred as the smallest contractile unit in heart muscle. The sarcomere comprises of three different myofilaments, namely the thin, thick, and elastic filaments (Fig. 2A). The thin filaments primarily consist of actin, along with other regulatory proteins such as tropomyosin and troponin, whereas the thick filaments consist of myosin. Cardiac contraction occurs by the pulling of thin filaments by the thick filaments toward the center of the sarcomere. This process relies on the heavily regulated cyclic interaction or crossbridge between thick and thin filaments.

During contraction, calcium binds to troponin C and transposes tropomyosin, revealing the myosin binding site on actin. This allows for actin binding by the myosin head and triggers conformational changes that cause the bending of the neck or the lever arm and subsequent sliding of thin filaments relative to thick filaments[3] (Fig. 2B).

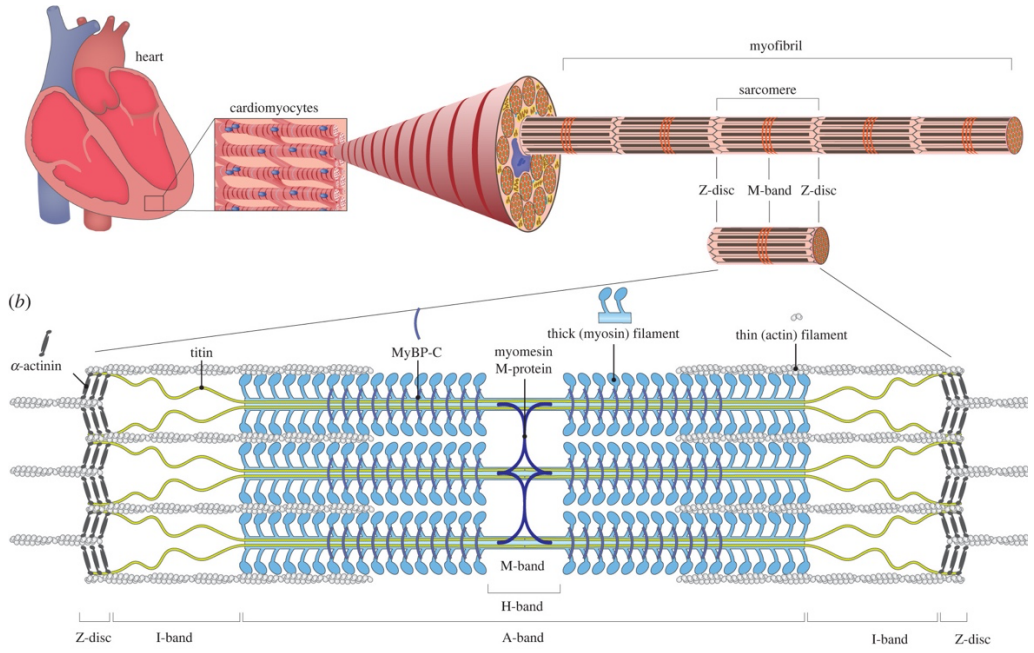


A)

B)

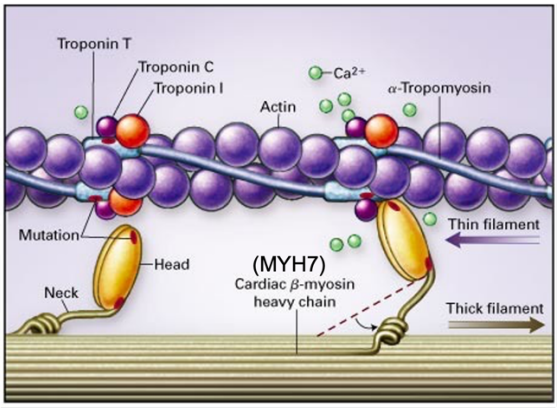


*Figure 2. A) Different level of cardiac muscle organization[4]. B) A power stroke generation by interactions between myosin and actin[3]. β-myosin heavy chain is encoded by MYH7 gene*

As myosin is important for the contraction of cardiac muscle, a disruption in any part of the myosin can significantly affect the structure function from protein to whole organ level. Approximately 30 to 50% of DCM cases are known to have a genetic basis[5]. These cases are referred to as familial or inherited DCM. Familial DCM can arise from missense mutation in multiple genes encoding for sarcomeric proteins, one of which is the MYH7 gene that encodes for β-myosin heavy chain (β-MHC, Fig. 2B).

A point mutation of arginine to glutamine at residue 369 (R369Q) in MYH7 gene was reported as an underlying cause of DCM in pediatric patient[5]. This residue is located at the tip of loop 4 of the upper 50kDa subdomain and directly interact with actin. This alteration replaces the positively charged residue with uncharged residue (Fig. 3)

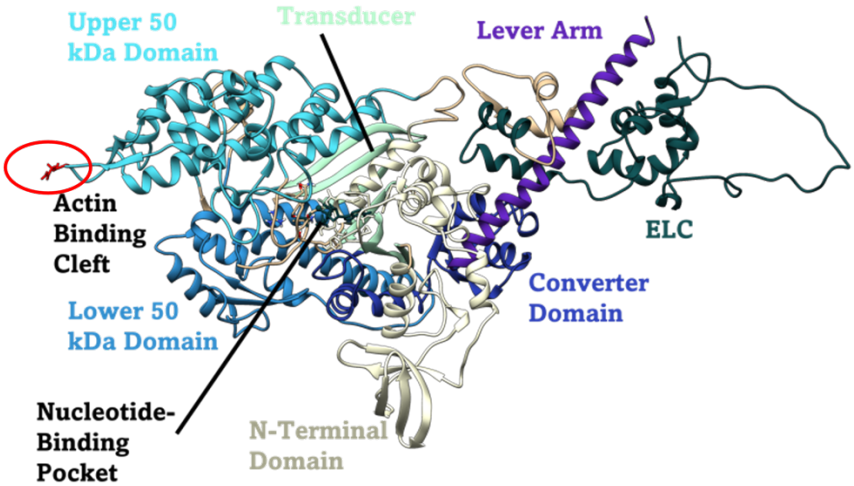


*Figure 3. Structure of the human β-cardiac myosin. The R369 residue is located at the actin binding cleft, as shown by the red circle. Illustration is provided by Aditi Prabhala*

Given the importance of actin-myosin interaction for cardiomyocyte contraction, the molecular implications of R369Q mutation are not well understood, including how the modification of crossbridge cycling leads to hypocontractility. As thin filament is regulated by calcium in exposing myosin binding site, calcium dynamics within an individual cardiomyocyte is crucial for its contraction and relaxation. Binding of myosin to actin cannot occur in absence of calcium although sufficient adenosine triphosphate (ATP), the primary chemical energy source, is present. In DCM, abnormalities in calcium handling within a cardiomyocyte may impact calcium transient and subsequent contractility. The precise mechanisms underlying these alterations are not fully understood and can vary among individuals.

**Calcium Regulation in Adult Cardiomyocytes**

Transient rises and reductions of cytosolic calcium ions ($Ca^{2+}$) in cardiomyocytes control each cycle of contraction and relaxation. It involves the release of $Ca^{2+}$ from the sarcoplasmic reticulum (SR) that is triggered by a transient rise in intracellular calcium levels. In the resting state, the SR contains a high concentration of calcium ions, while the cytoplasm has a relatively low concentration of calcium. When the heart muscle receives an electrical signal, an action potential is generated and propagates along the cell membrane (sarcolemma) and into the T tubules. The depolarization of the T-tubules leads to the opening of voltage-gated calcium channels, known as L-type calcium channels in the sarcolemma. The opened L-type calcium channels allows extracellular calcium to enter cardiomyocyte, resulting in a small increase in intracellular calcium concentration that triggers a conformational change in the ryanodine receptors (RyR). This causes the opening of these channels, allowing a larger amount of calcium to be released from the SR into the cytoplasm. This is known as calcium-induced calcium release. The released calcium ions bind to a protein called troponin C, which is part of the contractile apparatus within the cardiomyocyte. This binding initiates a series of molecular events that expose binding sites on actin, allowing myosin heads to bind and form crossbridges, as mentioned previously. Following contraction, the calcium ions are actively transported back into the SR by the sarcoplasmic reticulum calcium ATPase (SERCA), reducing the intracellular calcium concentration and allowing for muscle relaxation (Fig. 4).

The calcium-induced calcium release mechanism ensures that the rise in intracellular calcium is sufficient to activate the contractile proteins and initiate muscle contraction. The release of calcium from the SR amplifies the calcium signal that facilitates coordinated and synchronized

contraction of cardiomyocytes and leads to the pumping action of the heart. The regulation of calcium cycling in cardiomyocytes involves several other proteins and processes, such as calcium buffers, calcium pumps, and calcium extrusion mechanisms, which finely tune the calcium transient and ensure precise control over cardiac contraction and relaxation.

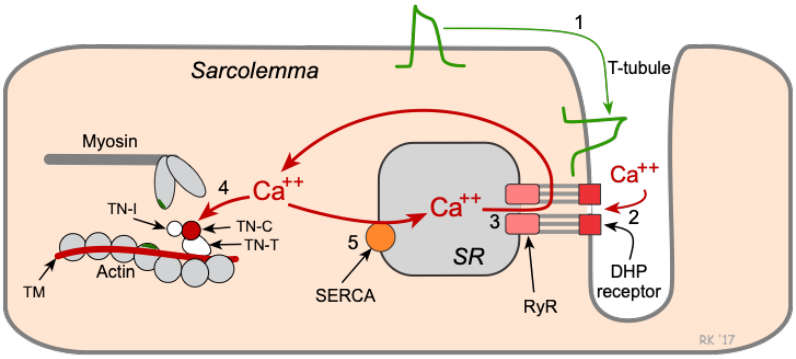


*Figure 4. Calcium handling process in cardiomyocytes[6]. $Ca^{2+}$ interacts with many molecular targets within the cardiomyocyte to facilitate contraction.*

**Myosin Crossbridge Cycle**

The contraction of the heart relies on the interaction between myosin-containing thick filament and actin-containing thin filament. During each heartbeat, myosin undergoes a series of molecular interactions that generate the necessary force for the contraction of cardiac muscle. MHC provides the structural framework for the myosin molecule and contains the regions responsible for binding to actin and ATP, which powers the contraction process. The MHC isoforms expressed in cardiac muscle differ from those found in other types of muscle, such as skeletal muscle. The specific isoforms expressed in the heart are tailored to meet the unique functional requirements of cardiac contraction, which is characterized by rhythmic and sustained contractions throughout an individual's lifetime.

The crossbridge cycle takes place in several step. At rest, the actin and myosin filaments overlap slightly but are not bound to each other. The myosin heads on the thick filaments are in a low-energy state, with ATP bound to them. The ATP bound to myosin is hydrolyzed into adenosine diphosphate (ADP) and inorganic phosphate (Pi), which re-energizes the myosin heads and prepares them for the next cycle (Fig. 5, step 1). When a cardiomyocyte receives a signal to contract, calcium ions are released into the muscle cell cytoplasm due to depolarization and activation of voltage-gated calcium channels. The rise in calcium concentration triggers a conformational change in the troponin-tropomyosin complex, exposing the active binding sites on

the actin filaments. The energized myosin heads bind to these sites, forming crossbridges between actin and myosin (Fig. 5, step 2). Once the myosin heads are bound to actin, they undergo a power stroke. This involves the release of inorganic phosphate (Pi) from the myosin head and a conformational change that causes the myosin head to pivot and pull the actin filament towards the center of the sarcomere (Fig. 5, step 3). This shortens the sarcomere, resulting in muscle contraction. After the power stroke, the myosin heads remain bound to actin and ADP detaches (Fig. 5, step 4). Then, ATP molecules in the cytoplasm bind to the myosin heads and causes the detachment of the myosin heads from actin (Fig. 5, step 5). The binding of ATP to myosin leads to a dissociation of the actin-myosin crossbridges. This allows the myosin heads to return to their low-energy state.

In addition to the crossbridge cycle (Fig. 5, step 1-5), myosin is also regulated through crossbridge recruitment by transitioning between "ON" and "OFF" myosin populations. The population of "ON" myosin are heads that are readily available to interact with actin (Fig. 5, step 6). The "OFF" state of myosin heads refers to heads that are sequestered along the backbone and not available to bind to actin (Fig. 5, step 7).

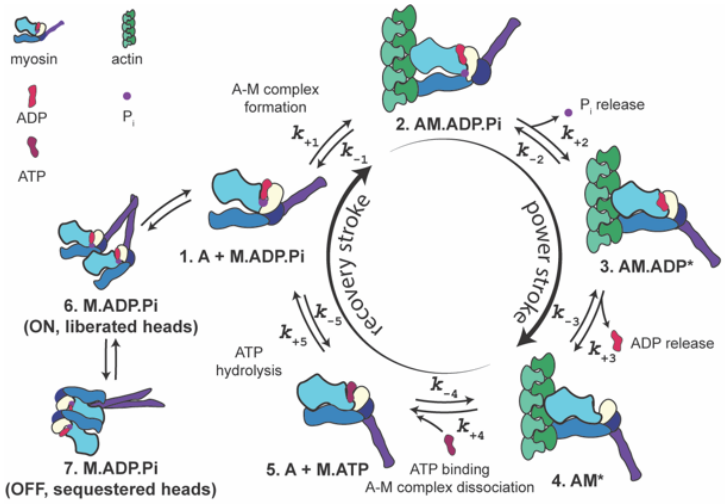


*Figure 5. The regulationon of myosin crossbridge. Myosin can bind to and detach from actin in a nucleotide-dependent manner. Illustration is provided by Dr. Matthew Childers.*

**Significance**

As the heart function depends on synchronous work of regulatory systems at different levels of complexity, *in vitro* molecular studies are critical for laying the foundation for the effects of R369Q mutations on myofilaments, sarcomere, and cell. Therefore, the purpose of this study is

to understand how MYH7 R369Q mutation alter the crossbridge cycle, specifically the rate of ATP binding to myosin, and cell contractility based on the calcium transient and sarcomere shortening.

Changes in ATP binding to myosin are crucial for the cyclic interaction between actin and myosin during muscle contraction. ATP binding allows for crossbridge detachment, ATP hydrolysis provides energy for the power stroke that generates force, and subsequent ATP binding resets the myosin heads for the next cycle. Consequently, modification of ATP binding rate to the myosin can impact the rate and extent of cardiomyocyte contraction and relaxation[7].

Sarcomere shortening is one of several parameters used to assess contractility. During contraction, the sarcomeres shorten as the actin and myosin filaments slide past each other, resulting in a reduction in sarcomere length. The greater the degree of sarcomere shortening, the stronger the contractile force generated by the muscle. Conversely, reduced sarcomere shortening indicates diminished contractile ability and may be indicative of hypocontractility.

By understanding the disease mechanism of DCM, researchers can identify specific targets or pathways that play a critical role in DCM. This information serves as a foundation for the development of targeted therapies aimed at modifying or reversing the disease process. Futhermore, as DCM is a heterogeneous disorder with various underlying causes and genetic factors, investigating the disease mechanisms helps identify subtypes or specific molecular signatures associated with DCM. This knowledge can pave the way for personalized medicine approaches, allowing tailored treatments based on the individual's specific disease mechanisms. It can also contribute to the development of biomarkers or diagnostic tools that aid in the early detection of DCM. It may also enable better prognostic indicators to assess the risk of disease progression and guide treatment decisions.

**Approach**

The are several challenges in studying DCM. First, obtaining an adequate number of DCM samples or models for research purposes can be difficult. Biopsy samples often yield variable mixture of wild-type or healthy and mutant myosin that differ from patients to patients. This can complicate the analysis of the effects of the mutation on heart muscle function. Second, DCM occurrence in patients are also affected by each individual’s background, such as genetic backgrounds, lifestyle, and environmental factor, which poses challenges in identifying common molecular pathways of DCM within a diverse patient population. Third, the widely used rodent model for cardiac research is also not ideal to study DCM, as they predominantly express α-MHC

chain isoform, rather than beta myosin heavy chain that is the primary isoform in human. It is specifically not ideal for studying R369Q mutation, as the mutation is in the gene that encodes β-MHC. Additionally, a prior study of pathogenic variants at the R369 residue was done using skeletal muscle from transgenic fruit fly model that did not resemble human cardiac muscle[8].

Over the past decade, human induced pluripotent stem cells (hiPSC) have been known as a powerful technology for cardiovascular research due to its capacity to be genetically engineered and differentiated into disease-relevant cardiomyocytes. hiPSC-CMs offer several advantages compared to other *in vitro* model, such as transgenic mouse and human biopsy samples. Though recent cardiomyopathy studies using transgenic mouse have provided insights into the disease pathogenesis, mouse ventricles express primarily α-MHC, not β-MHC like in the human heart[9]. Biopsy samples from end-stage DCM seem to resolve this issue; however, they are limited to small quantities and unknown ratios of wild-type or healthy to mutant proteins that can result in inconsistent observations[10]. hiPSC-CM is beneficial through its ability to recapitulate the native-like environment required for mutated proteins to reproduce the human cellular disease phenotype. This enables researchers to investigate the underlying molecular and cellular mechanisms of cardiac development, maturation, and function. They provide a controlled experimental system for studying factors that influence cardiomyocyte behavior, such as electrical properties, contractility, and response to external stimuli[9,11]. Taking these into considerations, wild-type isogenic control and CRISPR/Cas9-edited homozygous MYH7 R369Q hiPSCs are utilized for this project.

Differentiated hiPSC-CMs tend to resemble early fetal CMs with immature phenotype, including fetal sarcomere protein isoform, disorganized sarcomere structure, shorter sarcomere length, irregular cell shape, weaker force generation, lack of rod-shaped structure, and automaticity. To eliminate these fetal-like characteristics, different approaches have been done to enhance hiPSC-CM maturation. This project adapted the cell patterning method from Pruitt Lab at University of California Santa Barbara that enables control over cellular spatial organization and mimic the *in vitro* microenvironment with relevant physiological cues that lead to changes in morphology and function[12].

Following the hiPSC-CMs culture for 40 days, I isolated myofibrils to be used in stopped-flow spectroscopy to determine the rate of ATP binding to myosin. To observe calcium transient and sarcomere shortening through optics-based assay, the cardiomyocytes are cultured in patterned substrates to allow for single cell formation. By examining crossbridge formation, calcium

transient, and sarcomere shortening of cardiac cell harboring R369Q mutation, the altered molecular mechanisms of cardiomyocyte can be tethered to the overall impaired heart function at the tissue and organ levels.

## Methods

### hiPSC thawing and maintenance on 10 cm plastic tissue culture treated dish

The wild-type (WT) isogenic control and homozygous R369Q hiPSC lines were provided by the Allen Institute for Cell Science. They were derived from the ACTN2-mEGFP WTC line and CRISPR/Cas9-edited to express R369Q/R369Q mutation[13].

Prior to thawing and seeding hIPSCs, a 10cm polystyrene tissue culture treated dish was coated with 6 mL 0.17 mg/mL Growth Factor Reduced (GFR) Matrigel® dilution in DMEM/F12 media for at least 30 minutes in a tissue culture incubator at 5% $CO_2$ and 37˚ C. hiPSC cryovial was removed from liquid nitrogen and thawed quickly by gently swirling in 37˚ C water bath until only a small piece of frozen material remained. Each cryovial contained 0.5 to one million hiPSCs that was enough to be seeded in one 10 cm dish. 0.5 mL of warm culture medium that consisted of mTeSR1 and 10 μM Y-27632 Rho Kinase inhibitor (ROCKi) was gently added into the thawed cell suspension. The cells were transferred and resuspended into 10mL culture medium. Matrigel was aspirated from the tissue culture plate and the cell suspension was seeded into the plate. The medium was replaced with 10mL fresh mTeSR1 without ROCKi 24 hours after seeding.

The cells were fed daily with fresh mTeSR1 at room temperature until the cells reach 70-85% confluency or when the colonies approached the borders of the adjacent colony. Media dispensing and aspirating were done at the side of the vessel, allowing it to slowly cover the vessel surface without disturbing the cells. The colonies morphology was visually checked under bright field microscope at 10X or 20X magnification before changing the media. Good quality of hiPSC colonies were indicated by homogeneous appearing colonies with clear borders and absence of differentiated zones in the center of the colonies[14].

Monolayers of hiPSCs were detached from the 10 cm plastic tissue culture plate by washing them with DPBS and adding 3mL pre-warmed ACCUTASE™. Detachment occurred within three to five minutes of incubation in the 37˚ C incubator. To ensure all cells were released from the plate surface, the cell suspension weas gently rinsed with DPBS across the vessel and transferred into a conical tube. This process was repeated once before the cells were spun down at 1000 rpm for three minutes at room temperature. The supernatant was aspirated from the cell

pellets and resuspended in 7 mL mTesR1 that contained 10 μM ROCKi for seeding into a new 10cm tissue culture dish. To obtain specific plating number, 10 μL of the cell suspension was mixed with 10 μL Trypan Blue and applied to a hemocytometer. 300K cells were seeded into the new vessel with 10 mL media and fed with fresh mTeSR1 after 24 hours. hiPSCs were passaged at least twice post-thawing before starting differentiation into cardiomyocytes to fully recover cells from cryopreservation.

**Cardiomyocyte differentiation of hiPSCs on 12-well plastic tissue culture treated plate**

Directed differentiation of hiPSC to cardiomyocytes were performed in a monolayer platform through temporal modulation of Wnt signaling[15,16]. After three or four days of growth in 10 cm dish, the cells had mature morphology and were at an ideal density to be passaged to a new Matrigel-coated 10 cm dish and 12-well plastic tissue culture plate(s) for directed differentiation (DD). The culture process in 10 cm dish was carried out in the same process as mentioned above.

The cell seeding day was denoted as day -3 for DD plates The old mTeSR1 with ROCKi media was replaced with fresh mTeSR1 24 hours later or on day -2 and day -1 (Fig. 6). On day 0, the cells were at 60-70% confluency and ready for differentiation. mTeSR1 media was switched to warm RPMI/B27 minus insulin containing 7.5 μM CHIR99021. The RPMI/B27 minus insulin medium was obtained through mixing RPMI 1640 medium with insulin-free B-27™ supplement, which was expected to improve differentiation efficiency.

CHIR99021 is a highly selective glycogen synthase kinase 3 (GSK-3) inhibitor that acts as Wnt activator. Each well in a 12-well DD plate was given 2 mL medium and incubated for 48 hours. To inhibit Wnt processing and secretion on day 2, the media was replaced with 2 mL warm RPMI/B27 minus insulin containing 7.5 μM IWP 2 for each well. Since the addition of IWP 2 is time sensitive, the media was changed as close as possible to the 48 hours and the plate was promptly returned to the incubator. The media was changed into warm RPMI/B27 minus insulin on day 4 and RPMI/B27 plus insulin every 48 hours starting from day 6. Occurrence of spontaneous beating cells across the entire well was observed between day 6 and 14.

Efficient hiPSC-CMs expansion was done by replating cells in the most optimal well(s), where the visible beating percentage of the cell monolayer was between 50% and 90%, into new 12-well tissue culture plate(s). Each selected well was initially washed with 1mL DPBS and incubated with 0.5 mL TrypLE™ Select (10x) for 15 minutes at 37°C. If the cells had not detached after 15 minutes, the plates were gently shaken to help detaching the hiPSC-CMs and incubation

was repeated for up to 15 minutes to avoid toxicity. The process of cell dissociation from the culture plate was neutralized by adding the same amount of warm replating medium that consisted of RPMI-1640, B27 supplement plus insulin, Penicillin-Streptomycin (P/S), 5% Fetal Bovine Serum (FBS), and 10 μM ROCKi. Cell suspension was transferred to a 15- or 50-mL tube depending on the number of wells to replate and centrifuged at 1000rpm for five to seven minutes. After removing the supernatant, the cell pellets were resuspended with replating medium in a volume that is three times the number of replated wells. After Matrigel coating was removed, the cell solution was immediately added into the new wells and incubated for 24 hours. The media was changed to fresh RPMI/B27 plus insulin without ROCKi after 24 hours and every other day. Monolayer cell cluster formation was observed two to three days after replating.

Once hiPSC-CMs attached to the new plate and recovered from the replating process, they were metabolically purified by removing glucose from the growth medium and supplementing it with lactate. This was achieved by substituting RPMI-1640 with DMEM minus glucose media and 4mM sodium lactate for four to six days. hiPSC-CMs were still viable during this glucose deprivation period because they utilized metabolic pathways other than glycolysis, whereas non-cardiomyocytes required glucose for metabolism[17].

The purified hiPSC-CMs were given maturation media that contained 75% RPMI-1640, 25% DMEM minus glucose, and B27 plus insulin. The portion of DMEM in the media was gradually increased to better mimic the physiological condition of calcium. The maturation media was changed every other day until the culture process reached day 40.

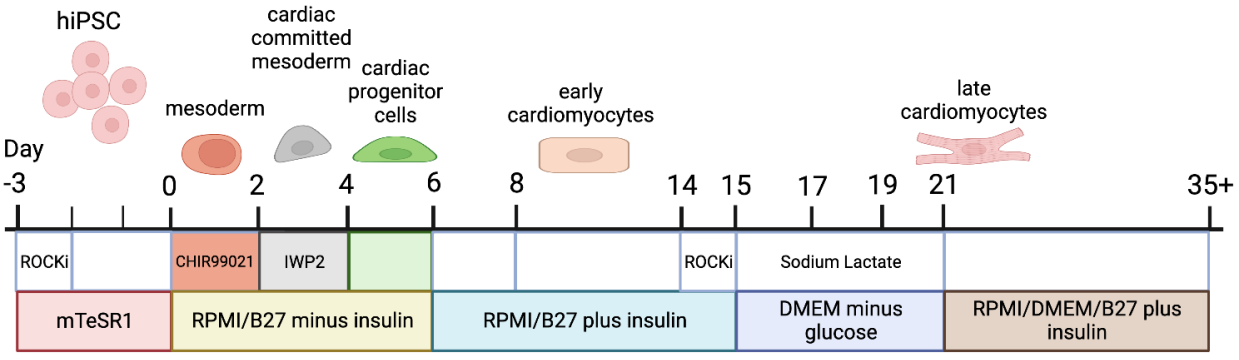


*Figure 4. DD proccess timeline. The different media and small molecules used at each stage are shown together with the markers that define the stage of differentiation.*

**hiPSC-CMs culture on micropatterned substrates**

The purpose of micropatterning hiPSC-CMs was to drive cell maturation and myofibril alignment that would be beneficial to accurately measure contractile output and calcium transient using an imaging system[12]. The micropattern stamp (microstamp) construction and hiPSC-CMs patterning techniques were adapted from Beth Pruitt Lab at University of California, Santa Barbara.

Patterning was attained using hiPSC-CMs that were at day 35 or later post-differentiation. The microstamp was manufactured using polydimethylsiloxane (PDMS) and a silicon wafer mold. Each microstamp area has a size of 1 cm x 1 cm and contained arrays of 1500-$\mu m^2$ rectangular features with an aspect ratio of 7:1. PDMS was poured onto the molds, cured at 60 °C, and peeled off the mold.

Each microstamp was initially washed with 100% ethanol and coated with 150 µL Matrigel solution at 4°C overnight. The coating solution consisted of Matrigel diluted to 1.0 mg/mL in DMEM/F12 media. On the patterning day, hiPSC-CMs were lifted using TrypLE and resuspended in replating solution as previously described to obtain a cell suspension with 300,000 cells/mL density. The microstamp pattern was transferred into a clean round glass coverslip with 25mm diameter through microcontact printing. Each coverslip was washed with 100% ethanol and Matrigel coating on each microstamp was aspirated and gently dried with $N_2$ gas. The microstamp was placed pattern-side down on the coverslip and pressed with 50 g weight for five minutes. After a 2-minute rest, the microstamp was carefully removed to ensure precise micropattern transfer. The coverslip was placed in a 12-well tissue culture plate well with the pattern facing up and ready to be used for cell culture.

150 µL of cell suspension was added into the pattern area and incubated at 37˚ C for 45 minutes. The cells were then given 3 mL solution containing RPMI, B27 plus insulin, and 10 µM ROCKi. The media was replaced with RPMI/B27 plus insulin after 24 hours and topped off with 2 mL solution two days after. Cells were seen to follow the shape of the micropattern 2 days post-seeding and ideal to be used for imaging-based experiment 5 days after seeding.

**Myofibril extraction from hiPSC-CMs starting at 37 days post-differentiation**

Mature hIPSC-CMs were harvested on day 37 or later via dissociation and extracted myofibrils were expected to predominantly consist of β myosin isoforms (Fig. 7). Data obtained by Kerry Kao, a graduate student in the Regnier Lab, demonstrated the separation of myosin

isoforms using SDS polyacrylamide gel electrophoresis. The results indicated that the myosin protein isolated from hiPSC-CMs at day 45 predominantly consists of β-MHC (Fig. 8).

Cell detachment was carried out in the same process as replating using TrypLE™ Select to obtain cell pellets. Depending on the size, resulting cell pellets were resuspended in a minimum 200 µL rigor buffer (50 mM Tris HCl, 100 mM KCl, 2 mM MgCl2, 1 mM EGTA, pH 7.2) and centrifuged at 2800 g for 10 minutes at 4 C. Once the supernatant was removed, the cell pellet was exposed for 1 hour to rigor buffer containing 0.5% Triton X-100 on ice. The skinned myofibrils were washed twice and resuspended in 200 µL rigor buffer to make the final suspension. The concentration of myofibrils was determined based on the $A_{280}$. The myosin content in the myofibril was assumed to be 40% and the myosin concentration was calculated using an extinction coefficient of 0.7 $(mg/ml)^{-1}$ $cm^{-1}$. Isolated myofibril was immediately used for the stopped-flow assay to avoid protein degradation.

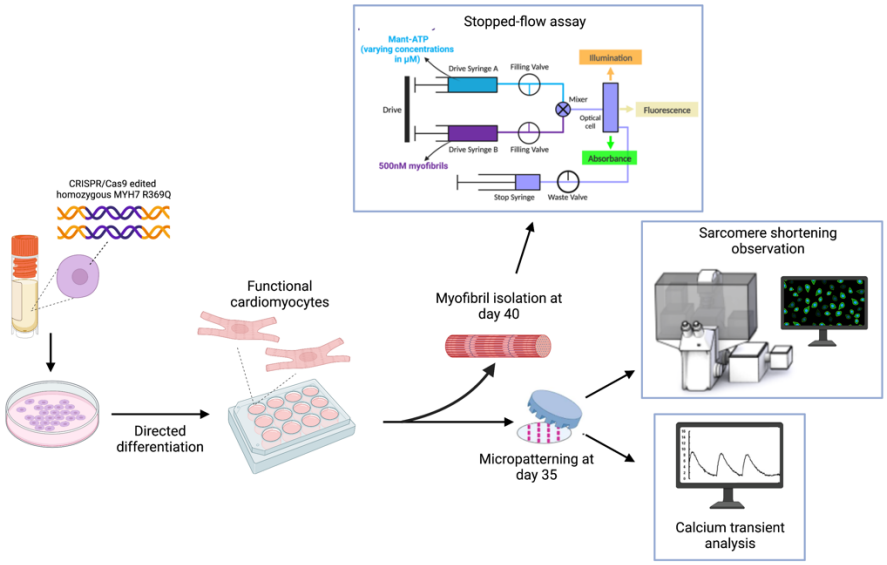


*Figure 7. Overview of the experimental process from differentiating hiPSC-CMs until performing structural and functional assays.*

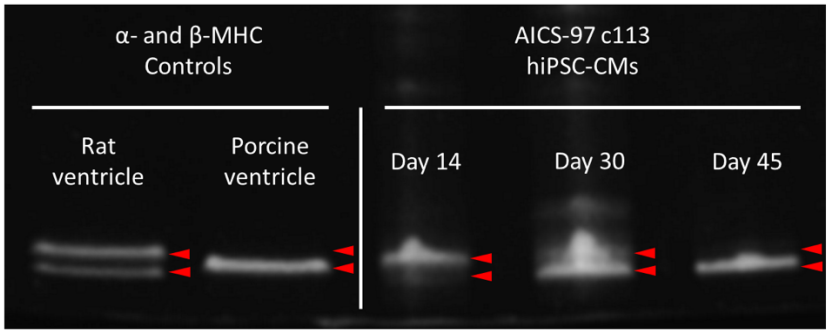


*Figure 8. MHC separation SDS-PAGE result. Rat ventricle predominantly has α-MHC and porcine ventricle predominantly has β-MHC. The band of myosin protein isolated from day 45 hiPSC-CMs is more aligned to that of porcine ventricle, indicating the MHC is mostly in β isoform. AICS-97 c113 is provided by the Allen Institute of Cell Science and derived from the same WTC11 background as R369Q hiPSC-CMs line.*

**Stopped-flow spectroscopy assay**

All stopped-flow experiments were conducted on a HiTech TgK Scientific DX stopped-flow spectrometer. The assay was performed using 20 /30 -O-(NMethyl-anthanoloyl)-ATP (mant-ATP) with its fluorescence was excited at 295 nm. Stock mant-ATP was diluted in rigor buffer to obtain 4 µM, 6 µM, 8 µM, and 10 µM mant-ATP. Isolated myofibril was also diluted in rigor buffer to achieve a working concentration of 500 nM.

The stopped-flow assay was run using two coupled syringes, one of which contained the 500 nM myofibril and the other contained mant-ATP in varying conditions. When driven together in a single shot setting, the solution in each syringe flowed together and rapidly mixed in the observation chamber. The injected volume was limited by the stop syringe which provides the "stopped-flow". The resulting fluorescence percentage from mant-ATP binding to myosin was recorded within 10 seconds of recording. A minimum of five traces were collected to obtain an average trace using Kinetic Studio program. Each average fluorescence curve was fitted using second-order exponential equation to gain the kinetic value based on the resulting slope.

**Calcium imaging of patterned hiPSC-CMs ionoptix**

Calcium transient of WT and R369Q mutated hiPSC-CMs was analyzed using the IonOptix Calcium and Contractility System. hiPSC-CMs that had been patterned for six days were loaded with 0.15 µM ratiometric calcium indicator, Fura-2 acethoxymethyl (AM) ester. 50 µg of Fura-2 AM powder was diluted in 50 µL DMSO to make 1 mM Fura-2 AM solution. This solution was further diluted in warm RPMI/B27 media to reach 2.67 µM for easier Fura-2 AM addition into the tissue culture well. Once the AM ester was added, the cell was incubated at 37˚ C for 15 minutes

and the media was replaced with warm RPMI/B27 plus insulin and incubated for another 15 minutes. Fura-2 AM was prepared in the dark, as the compound is light sensitive.

The glass coverslip containing Matrigel-micropatterned WT or homozygous R369Q hiPSC-CMs was placed on the stage and perfused with warm Tyrode's solution (1.8 mM $CaCl_2$, 1.2 mM $MgSO_4$, 3.7 mM KCl, 138 mM NaCl, 1.2 mM $KH_2PO_4$, 10 mM HEPES, 5 mM Glucose, pH 7.36). The cells were paced with 1 Hz field stimulation at 37°C using MyoPacer field stimulator (15V, 4ms). Motic AE31 microscope and Olympus UApo/340 40x objective lens were used to select a healthy single cardiomyocyte following the pacing. To start recording, the selected cell was aligned horizontally and the cell framing adapter was adjusted to minimize background area. Cells were able to be paced for approximately 40 minutes. The acquired calcium transient traces were analyzed with IonWizard software to obtain time to 50% peak/baseline, time to 90% peak/baseline, time to peak, departure velocity, and return velocity relevant parameters.

**Live cell imaging**

α-Actinin (ACTN2) is the predominant protein in the sarcomere z-disk. The GFP-tagged ACTN2 facilitated sarcomere shortening observation using live cell inverted widefield/spinning disk confocal microscope in Lynn & Mike Garvey Imaging Core at University of Washington Institute for Stem Cell and Regenerative Medicine. 40 days after onset differentiation, WT and R369Q homozygous hiPSC-CMs were cultured on patterned 6-well glass bottom tissue culture plate and imaged 6 days later (46 days total after the onset differentiation). The plate was mounted in an environmental chamber for acquisition at 37°C and 5% $CO_2$.

All images were collected with a Yokogawa W1 spinning disk confocal on a Nikon Eclipse-TI inverted microscope (Nikon) equipped with a PLAN APO-40x objective and 1.5x magnification. ACTN20-EGFP fluorescence was excited with the 488nm laser (Alexa488 fluorescence emission filter) at 50% transmission. Images were acquired with NiS-Elements controlled camera using an exposure time of 50 ms. Brightness and contrast were adjusted on displayed images using NIS-Elements software. The resulting videos were analyzed with Fiji, a distribution of ImageJ software, and SarcOptiM plug-in to quantify sarcomere shortening. SarcOptiM computed sarcomere length via Fast Fourier Transform (FFT) analysis of video frames displayed in ImageJ.

For each video of contracting hiPSC-CMs, selection of the cardiomyocyte longitudinal axis was done by positioning a line from one z-line to another parallel z-line. ImageJ then computed a

grey level profile that followed the sarcomere striation profile. FFT spectrum of the profile and peak value range were defined by user-input minimum and maximum sarcomere length of 1 and 4 μm. The corresponding sarcomere length based off the pixel size that changed over the video time course[18]. The fraction of sarcomere shortening was calculated by dividing the difference between the length at rest and length at peak contraction by resting length multiplied by 100%.

**Statistical analysis**

GraphPad Prism was used for statistical analysis and graphing. Simple linear regression through the origin was used to determine the association between two continuous variables. The $r^2$ value was estimated using nonlinear regression. $R^2$ value closer to 1 indicates that the data perfectly fit the linear model. Unpaired t test was used to compare the difference between two groups, and $P < 0.05$ was considered to be significant. The values shown in the bar graphs are means ± SEM.

## Results

**Optimization of hiPSCs directed differentiation (DD) into cardiomyocytes**

hiPSCs are directed towards a cardiac lineage by exposing them to specific signaling pathways and growth factors. The differentiation yield of hiPSC is affected by the quality of the matrix, media, small molecules, cell density and cell confluency[11,12]. Appropriate cell density is known to be cell line- and vessel size-dependent. Both WT and homozygous R369Q hiPSC were initially seeded into 12-well tissue culture plate in 100K, 125K, and 150K cells/$cm^2$ densities for DD. mTeSR1 cell culture medium was given for two days to provide enough time for the cells to recover and reach a confluency of 70 – 85%. This first iteration resulted in unsuccessful differentiation, as there were still undifferentiated colonies with compact, tightly packed cells and lacked of morphological changes (Fig. 9A). Clusters of beating cells were seen in wells with 100k cells/$cm^2$ density, yet it was suboptimal.

This observation could have been attributed to excessive cell confluency in all wells upon the addition of CHIR99021 on day 0 of differentiation. Without changing the CHIR99021 concentration, cell seeding density was subsequently decreased by half to reduce the cell confluency to be around 50-60% on day 0. This approach appeared to be effective for WT and R369Q homozygous clone in three different cell densities (Fig. 9B). Beating cardiomyocytes were seen on day 6 and spontaneous contraction of larger areas were seen between day 8 and 10.

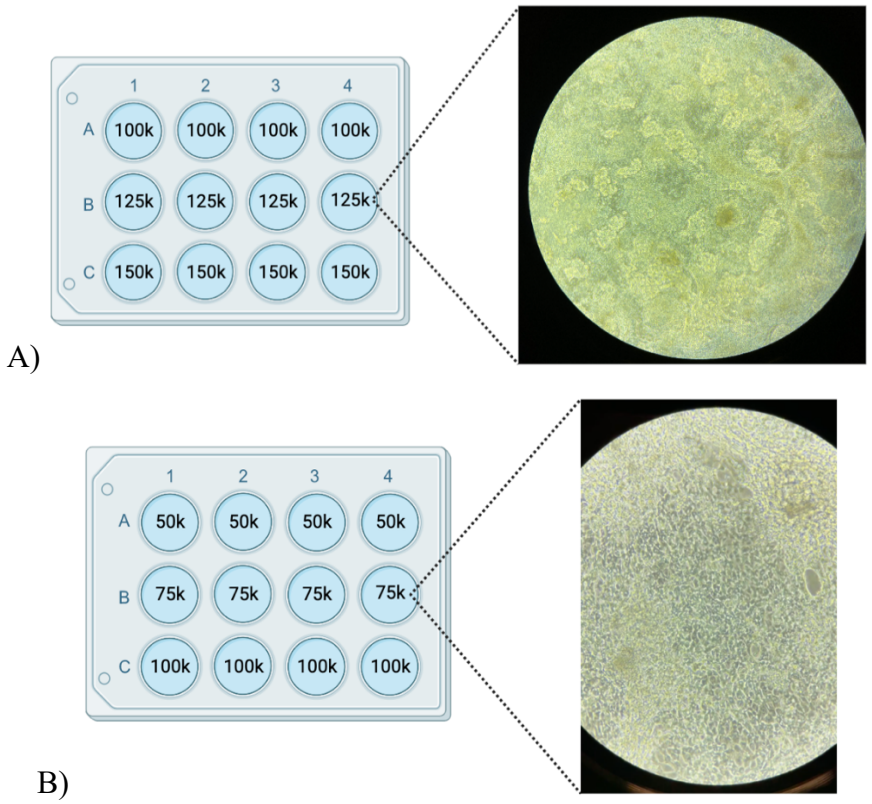


*Figure 9. A) Schematics of DD plate with varying cell seeding densities that resulted in excessive confluency and undifferentiated cell colonies. Cellular beating, if observed at all, was limited to small clusters and displayed a patchy pattern. B) Schematics of DD plate with lower cell seeding density and the resulting hiPSC-CMs with 30-50% purity. These hiPSC-CMs are observed to beat synchronously as a monolayer.*

**hiPSC-CMs culture on patterned substrates**

The purpose of patterning hiPSC-CMs is to guide their spatial organization and create more physiologically relevant cardiomyocytes monolayer. In order to promote the mature alignment of myofibrils in individual hiPSC-CMs, they were cultured on patterned round glass coverslips or glass-bottom tissue culture plate for 6 days starting from day 35 or later. This strategy was also beneficial to improve contractile function and electrophysiological properties[12]. Expression of ACTN2-mEGFP in WT and homozygous R369Q cells enable the visualization of sarcomeric z-line. In glass-bottom tissue culture plates without any patterning, the hiPSC-CMs exhibited a disorganized arrangement, and the myofibrils showed random orientation (Fig. 10A, B). Following the application of a Matrigel line micropattern with 15 μm width and 5000 μm length on the glass

surface, the cells exhibited a more consistent and aligned arrangement. The Z lines were seen between adjacent sarcomeres perpendicular to the direction of myofibril alignment (Fig. 10C, D).

In terms of contraction, the unpatterned hiPSC-CMs exhibited a spontaneous and irregular rhythm in uncoordinated manner throughout the tissue culture well. The patterned hiPSC-CMs had more synchronous contraction, mimicking the behavior of cardiomyocytes in native cardiac tissue.

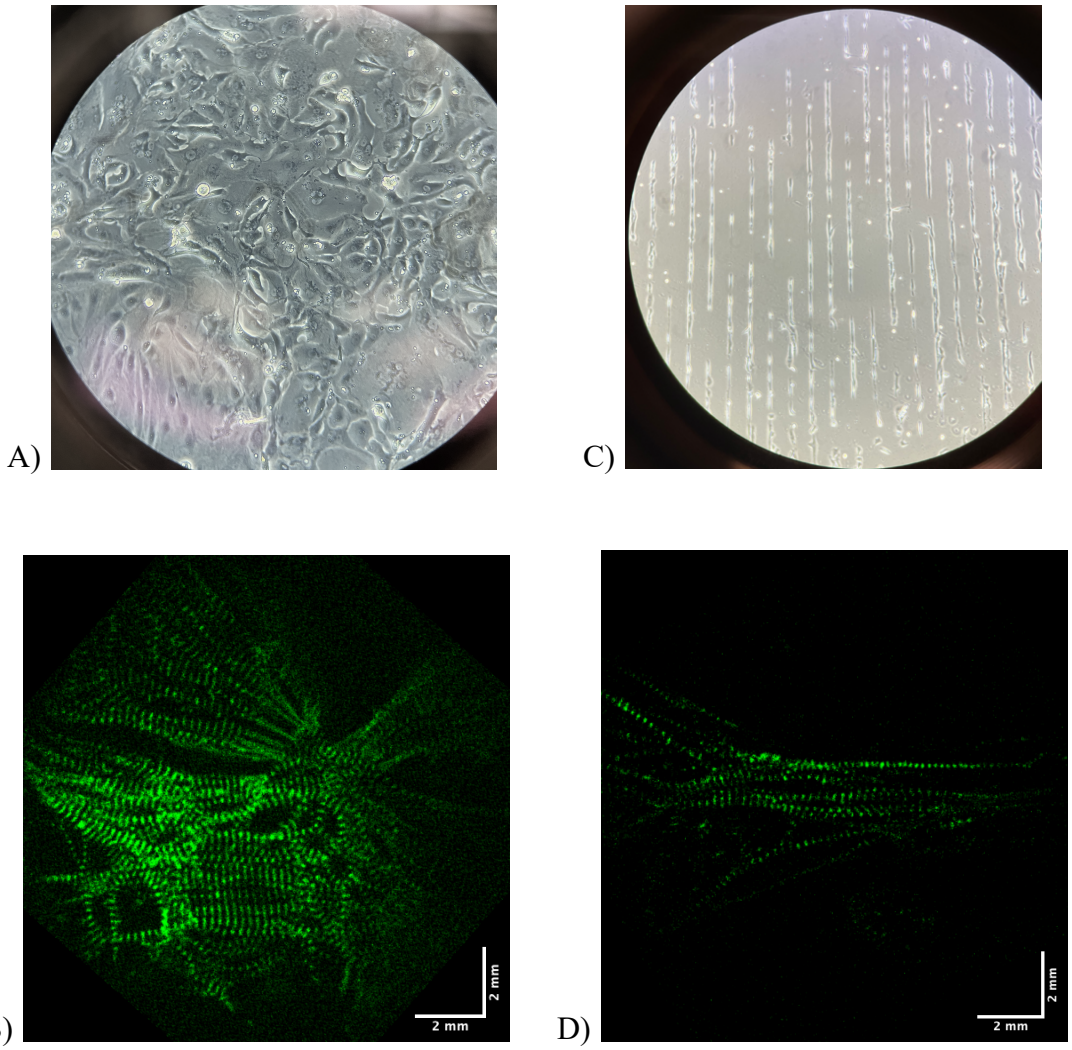


*Figure 10. Representative image of unpatterned and patterned hiPSC-CMs structures and myofibrils alignment. A) hiPSC-CMs exhibited irregular shapes and sizes and lacked organized structures when cultured in unpatterend glass-bottom tissue culture plate. B) Fluorescent labeling of z-lines of unpatterned hiPSC-CMS showed random directionality. C) hiPSC-CMs were seen to elongate uniformly following the line pattern after seeded into a patterned glass coverslip or glass-bottom tissue culture plate. D) Fluorescent labeling of z-lines of patterned hiPSC-CMS showed uniform alignment and elongated myofibrils. All images were WT cells taken on day 46- or 6-days post-cell patterning. Image A) and C) were taken with brightfield microscope at 10x. Image B) and D) were taken with live cell inverted/spinning disk confocal microscope.*

**Observation of Mant-ATP binding rate to healthy and homozygous R369Q hiPSC-CMs using stopped-flow spectroscopy**

To assess the rate of ATP binding to WT or homozygous R369Q hiPSC-CMs myosin, myofibrils from each clone in rigor was rapidly mixed with Mant-ATP in stopped flow spectroscopy. The fluorescent transients were previously described by a double exponential as the binding of Mant-ATP to myosin was a summation result of fast and slow phase. The fast and slow phase is correlated with the "ON" state of myosin head and "OFF" myosin head respectively[21]. The comparison focused exclusively on the rate constants derived from the fast phase, as they hold greater physiological relevance. Further elaboration on this topic will be provided in the discussion section.

For each measurement, six transients were collected to generate an average. The rate constant of ATP binding to WT myofibrils were comparable to unpublished data from other hiPSC-CMs lines generated from WTC11 background. Increasing concentration of Mant-ATP resulted in increasing fluorescence percentage with retained curve shape (Fig. 11A). A plot of $k_{obs}$ vs. concentration of Mant-ATP over a range of 2 to 5 µM reveals a linear relationship between the two variables. The slope of this relationship, the second order rate constant, is related to the ATP binding rate. The rate constant for ATP binding to R369Q myofibrils is found to be approximately halved as the healthy myofibril, as shown by the less steep slope (Fig. 11B).

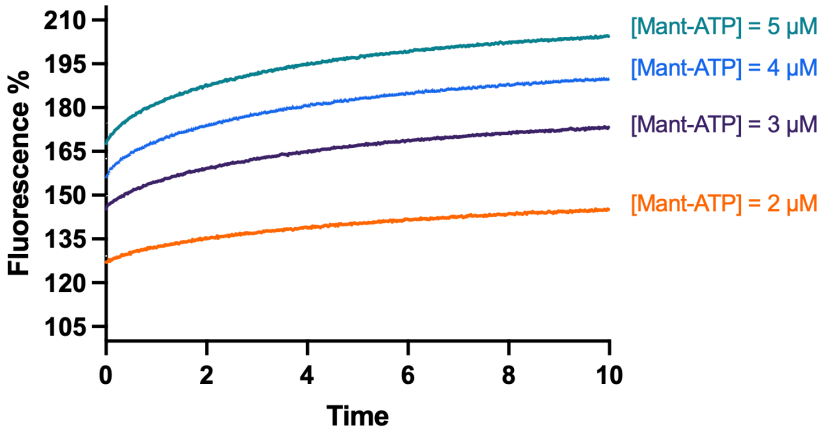


A)

B)

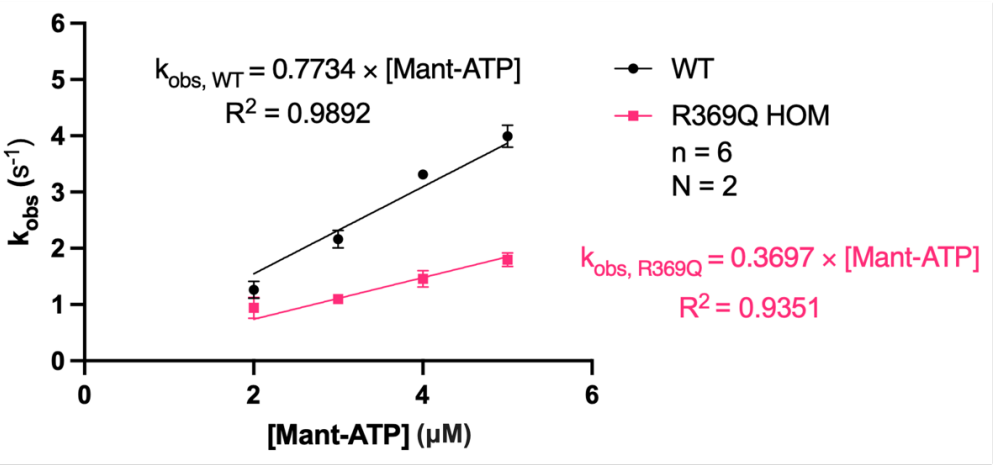


*Figure 11. Measurement of the association rate constant of mantATP. A) Representative average of fluorescence signal change upon mixing Mant-ATP with 500 nM myofibrils. The fluorescent change amplitude increases as the Mant-ATP concentration increases. The data is fit to double exponential function B) Rate constants ($k_{obs}$) for the reaction of mantATP with rigor WT or homozygous R369Q myosin plotted against concentration of mant-ATP.*

**Quantification of sarcomere shortening percentage based off the expression of ACTN2-EGFP**

Contractility of micropatterned WT and homozygous R369Q hiPSC-CMs were assessed at day 51. Sarcomere shortening of was measured on live-cell video that captured changes in distance between two z-lines based off the expression of ACTN2-EGFP during cell contraction and relaxation (Fig. 12A). A minimum of 15 sarcomere length traces was recorded to obtain well-defined average. The average sarcomere length is 1.95 μm for healthy cells and 2.02 μm for homozygous R369Q cells at rest (Fig. 12B). The average minimum sarcomere length during contraction is 1.65 μm for healthy cells and 1.83 μm for homozygous R369Q cells (Fig. 12C)
The fractional shortening, a measure of contractile function, was higher in WT hiPSC-CMs with a change of 15.2%, while the R369Q cells exhibited a lower contraction-induced shortening of 9.3% (Fig. 12D). The obtained data suggests that diminished contractility in DCM heart is confirmed by reduced fractional shortening observed in homozygous R369Q hiPSC-CMs.

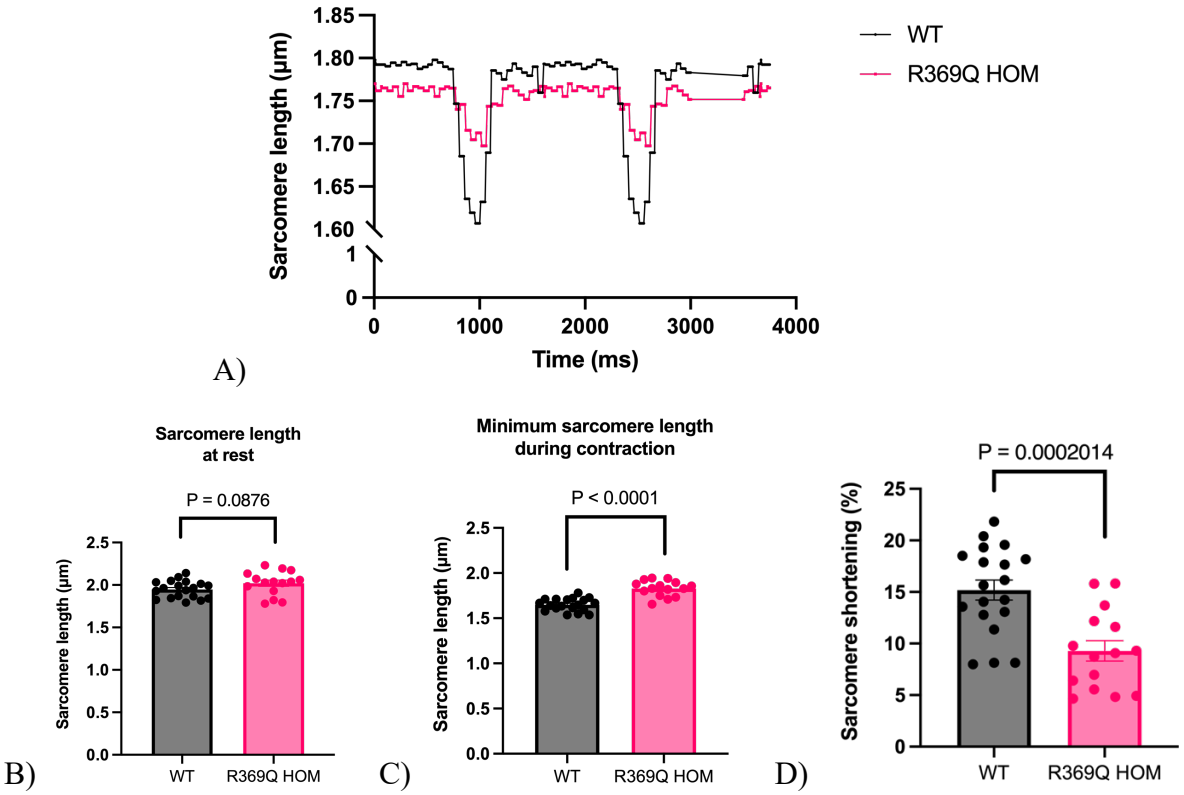


*Figure 12. A) Example of sarcomere shortening trace of one WT and one homozygous R369Q cardiomyocyte without external electrical stimuli (unpaced) at similar beat rate. B) Average of sarcomere length at rest. C) Average of maximum sarcomere length during contraction. E) Corresponding fractional shortening or percentage of sarcomere shortening.*

**Calcium transient analysis**

*In vitro* $Ca^{2+}$ handling properties were evaluated by measuring the amplitude and kinetics of $Ca^{2+}$ transients recorded from Matrigel micropatterned hiPSC-CMs on cover glass loaded with Fura-2 AM. All cells were given an external electrical stimulus (pacing) at 1Hz. Based on the normalized calcium transients, healthy and homozygous R369Q hiPSC-CMs exhibit similar transient. (Fig. 13A). This is supported by the quantification of the time to 50% peak (Fig. 13B), 90% peak (Fig. 13C), 50% baseline (Fig. 13D), 90% baseline (Fig. 13E), and the peak amplitude (Fig. 13F). In this analysis, data is considered statistically significant when the p-value is less than or equal to 0.05 ($p \leq 0.05$).

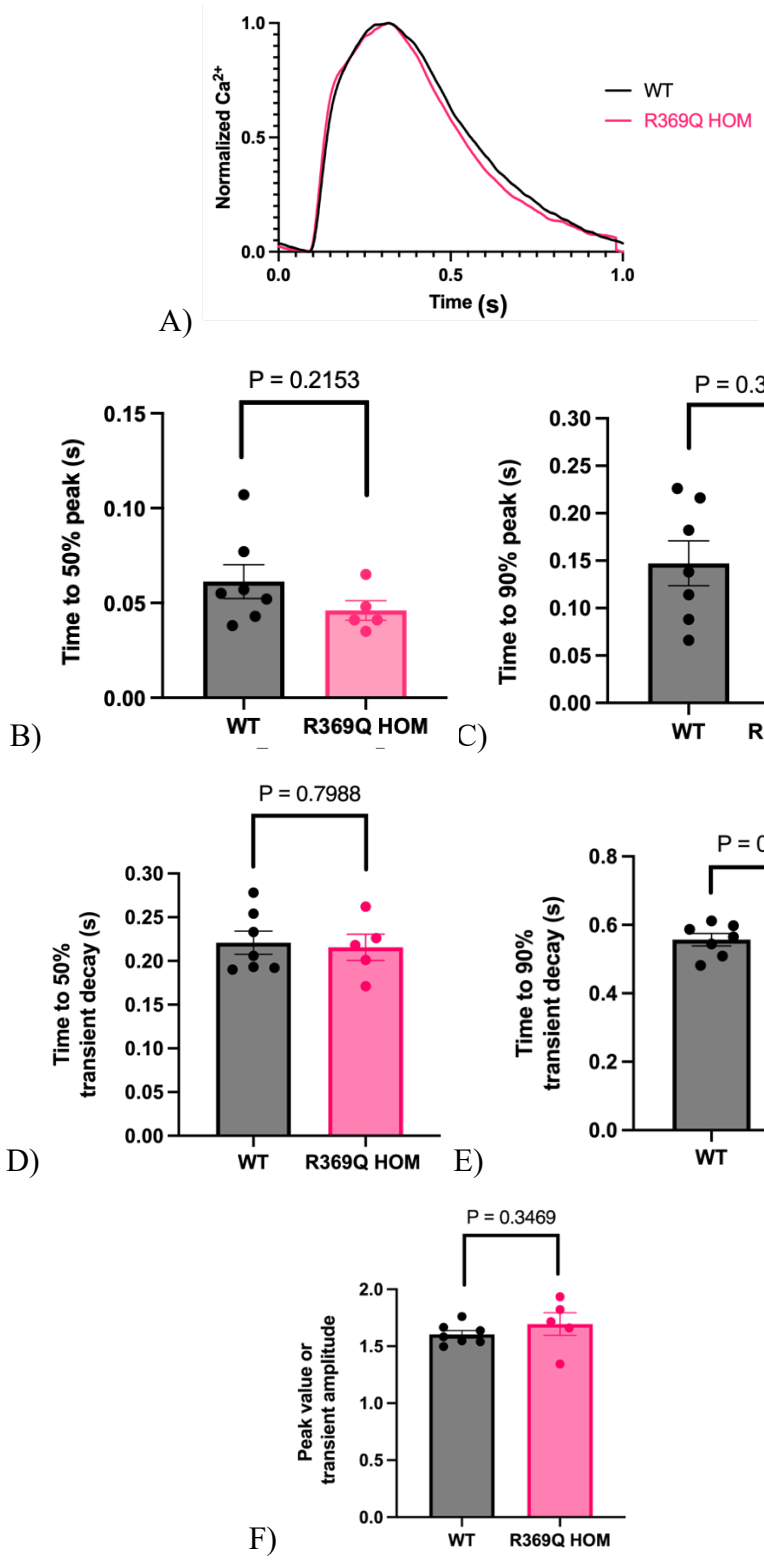


*Figure 13. A) Normalized $Ca^{2+}$ transients of healthy and homozygous R369Q hiPSC-CMs. B) time to 50% peak, C) time to 90% peak, D) time to 50% baseline, E) time to 90% baseline. Average traces are made of n=7 for WT and n=5 for homozygous R369Q hiPSC-CMs.*

## Discussion

Abnormalities in the myosin crossbridge kinetics or calcium handling can lead to contractile dysfunction in hiPSC-CMs. Dysregulation of calcium handling can affect the magnitude and duration of the calcium transient, leading to impaired crossbridge activation and relaxation. To model the impacts of the R369Q mutation in these scenarios, CRISPR-edited hiPSC-CMs were utilized.

### hiPSC seeding density impacts the quality and functionality of the differentiated cardiomyocytes

In this study, the tissue culture protocol was optimized by reducing the cell density to half of the recommended value. The WT and R369Q homozygous clones used in this project were 50-70% confluent within 2-3 days, resulting in successful hiPSC differentiation into beating cardiomyocytes with high purity that were viable for downstream functional assays. Cell density has a significant impact on the efficiency, quality, and functionality of the differentiated cardiomyocytes. As differentiation depends on signaling cascades, optimizing cell density may affect the interactions and communication between neighboring cells. With higher cell density, the concentration of molecules that drives the activation and inhibition of Wnt signaling pathways may be insufficient and fail to promote the desired lineage specification. Cell density also impacts the availability of nutrients and oxygen within the culture system. As cells proliferate and differentiate, their metabolic demands increase. Insufficient nutrient and oxygen supply due to high cell density can lead to cellular stress, compromised viability, and impaired differentiation.

### Micropatterning allows precise control over the spatial arrangement and organization of hiPSC-CMs

Multiple attempts have been made to obtain mature hiPSC-CMs that closely resemble adult human cardiomyocytes, including physiological shape[12]. Micropatterning can promote the maturation of hiPSC-CMs by providing spatial cues that mimic the native cardiac microenvironment. By aligning hiPSC-CMs in a specific pattern, the cells have more organized myofibrils, improved sarcomere alignment, and enhanced electromechanical coupling. This can lead to hiPSC-CMs exhibiting more mature contractile properties and electrical behavior, as well as β-MHC isoform that resemble adult cardiomyocytes.

Additionally, micropatterning hiPSC-CMs offers several benefits for single cell visualization. By confining cells to defined patterns or microstructures, the morphology and changes of individual cells can be easily identified and tracked. This is particularly useful for observing sarcomere shortening with minimized cell-cell overlap. Patterning also promotes uniformity in cell shape and organization, which can enhance imaging and analysis techniques. It allows for consistent imaging conditions and reduces experimental variability arising from variations in cell shape and orientation.

**Myosin with R369Q mutation exhibits slower ATP binding**

The R369Q homozygous mutation was shown to have a slower ATP binding rate to myosin. This result contradicts the decreased contractility hypothesis for DCM caused by mutation in β-MHC. When ATP binding is slower, the myosin heads stay attached to the actin filaments for a longer period of time. A possible explanation for the slower ATP binding rate of R369Q mutation may rely on the thick filament regulation and mechanisms that control the number of available myosin heads to interact with actin and generate power stroke (Fig. 4).

Over the past decade, a multitude of studies have contributed to our understanding of the ON state and OFF state of myosin. Throughout muscle contraction process, myosins undergo a constant transition between the actin-bound state and the actin-free ON state. In OFF state, myosins remain "in-reserve" and do not actively contribute to contractility. In both cardiac muscle fibers, 50-60% of myosin heads are estimated to exist in the OFF state, suggesting their role as non-participants in the contraction process[22]. OFF state was hypothesized to occur in two states, traditional interacting-head motif (IHM) or a non-IHM state. IHM refers to two myosin heads that pack together during relaxation and limit their potential interaction with actin[22, 23].

A human β -cardiac myosin quasi-atomic model created by Alamo et. al. reveals that R369Q mutation stabilizes the position of actin-binding myosin head to dock onto its own S2[23]. This may suggest that fewer myosin head will be available to bind to ATP and therefore the binding rate is slower than healthy cardiomyocyte. Incorporation of the OFF state in experimental investigations of the R369Q mutation may unveil valuable insights into the mechanisms underlying the development of hypocontractility in DCM.

The decreased contractility caused by R369Q mutation may be attributed to compensatory changes in subsequent steps of the ATP binding process within the crossbridge cycle. For instance, the ATP turnover rate provides important information about the dynamics and efficiency of the

crossbridge cycle during muscle contraction. Considering that R369 residue is situated at the interface with actin, examining the actin binding rate to myosin can provide valuable insights into potential changes within the crossbridge cycle.

In the context of ATP-binding experiments, myofibrils were utilized with deactivated thin filaments, indicating that the actin sites on the thin filaments were unavailable for myosin binding. Studying myosin without regulated thin filaments may not fully reflect the physiological conditions of the heart, where actomyosin interactions play a crucial role in muscle function.

**Reduced fractional shortening of R369Q sarcomeres confirms the hypocontractility feature of DCM**

The average resting sarcomere length of both WT and homozygous R369Q was found to be similar to that observed in a functional human heart, ranging from 1.8 to 2.2 μm. The WT sarcomere length during contraction was also found to be comparable to that of the human heart, measuring approximately ~1.7 μm[24]. Fractional shortening, which represents the percentage of ventricular chamber contraction during systole, serves as an essential parameter for evaluating cardiac contractile function. The decreased fractional shortening or sarcomere shortening percentage observed in the R369Q mutation provides strong evidence supporting the presence of hypocontractility, a characteristic commonly associated DCM. This observation can also be attributed to a decrease in the number of active myosin heads, which in turn leads to reduced force generation by the motor.

It is important to consider that hiPSC-CMs are cultured on a rigid glass surface, which possesses a stiffness of approximately 70 GPa, in stark contrast to the relatively softer human heart tissue (~10 kPa). hiPSC-CMs on glass experience a stiff mechanical environment, which can affect their ability to generate force and contract. In some cases, the high stiffness of the glass surface can lead to multiphasic contractile forces in cardiomyocytes[23]. Nevertheless, hiPSC-CMs that exhibited multiphasic contractility was excluded from the analysis. One approach to address this issue is to utilize a more pliable substrate, such as a polyacrylamide gel with a stiffness that approximates the physiological levels. The gel will provide a more realistic mechanical environment for hiPSC-CMs that potentially influence their maturation and function[26].

**Calcium transients between healthy and homozygous R369Q cardiomyocytes are not significantly different**

There is no significant difference observed in the calcium transient comparison between healthy and mutant cardiomyocytes. This may suggest that R369Q mutation primarily cause crossbridge cycling or recruitment issues, rather than calcium handling problems in cardiomyocytes.

During a calcium transient, the calcium concentration typically rises rapidly to a peak value and then gradually returns to its baseline level. A shorter time to 90% baseline indicates a faster decline in the calcium concentration in the cytoplasm. Accelerated calcium sequestration can disrupt normal calcium signaling pathways, affecting downstream signaling cascades and cellular responses. Furthermore, if calcium is sequestered too rapidly from the cytoplasm, it can interfere with the availability of calcium ions for the activation of contractile proteins, leading to impaired muscle contraction and reduced contractile force.

Relying solely on calcium transient analysis may not be sufficient to draw definitive conclusions. Additional analyses and investigations are needed to provide a more holistic view about calcium handling in R369Q cardiomyocytes. This may include studying other molecular and cellular processes, such as gene expression, protein interactions, cellular structure, and signaling pathways. One additional constraint of this experiment is the uncertainty surrounding the extent of MHC isoform switching from α-MHC to β-MHC, as measurements were not conducted on all hiPSC-CMs. Therefore, it is possible that there are cells within the sample that exhibit immature calcium handling capabilities.

## Future Work

To summarize, the expression of the homozygous R369Q mutation in hiPSC-CMs results in reduced contractility, as evidenced by decreased sarcomere shortening. The slower ATP binding to R369Q myosin may be explained by the reduced number of available myosin heads for this process. Regarding calcium regulation, the calcium transient observed in R369Q cardiomyocytes does not indicate any abnormalities, as it closely resembles that of healthy cardiomyocytes.

A more comprehensive experimental investigation is required to uncover the mechanisms underlying DCM at various levels of heart organization. It would be beneficial to incorporate actin into the experimental system to investigate the kinetics and force generation of

cardiomyocytes comprehensively. Assessing myosin motility would also provide advantages in evaluating the overall efficiency of the crossbridge cycle. Additionally, further studies should explore contractility using various parameters, such as quantifying force generation and assessing calcium sensitivity.

References


1. Weintraub, R. G., Semsarian, C., & Macdonald, P. (2017). Dilated cardiomyopathy. *Lancet*, *390*(10092), 400–414. https://doi.org/10.1016/s0140-6736(16)31713-5
2. *Dilated Cardiomyopathy (DCM)*. (n.d.). Org.Nz. Retrieved May 26, 2023, from https://www.cidg.org.nz/patients-families/cardiac-inherited-diseases/dilated-cardiomyopathy-dcm/
3. Kamisago, M., Sharma, S. D., DePalma, S. R., Solomon, S., Sharma, P., McDonough, B., Smoot, L., Mullen, M. P., Woolf, P. K., Wigle, E. D., Seidman, J. G., & Seidman, C. E. (2000). Mutations in sarcomere protein genes as a cause of dilated cardiomyopathy. *The New England Journal of Medicine*, *343*(23), 1688–1696. https://doi.org/10.1056/NEJM200012073432304
4. Ahmed, R. E., Tokuyama, T., Anzai, T., Chanthra, N., & Uosaki, H. (2022). Sarcomere maturation: function acquisition, molecular mechanism, and interplay with other organelles. Philosophical Transactions of the Royal Society of London. Series B, Biological Sciences, 377(1864), 20210325. https://doi.org/10.1098/rstb.2021.0325
5. Dellefave, L. M., Pytel, P., Mewborn, S., Mora, B., Guris, D. L., Fedson, S., Waggoner, D., Moskowitz, I., & McNally, E. M. (2009). Sarcomere mutations in cardiomyopathy with left ventricular hypertrabeculation. Circulation. Cardiovascular Genetics, 2(5), 442–449. https://doi.org/10.1161/CIRCGENETICS.109.861955
6. CV Physiology. (n.d.). Cvphysiology.Com. Retrieved May 21, 2023, from https://cvphysiology.com/Cardiac%20Function/CF022
7. Barrick, S. K., & Greenberg, M. J. (2021). Cardiac myosin contraction and mechanotransduction in health and disease. *Journal of Biological Chemistry* , *297*(5). https://doi.org/10.1016/j.jbc.2021.101297
8. Trujillo, A. S., Hsu, K. H., Viswanathan, M. C., Cammarato, A., & Bernstein, S. I. (2022). The R369 Myosin Residue within Loop 4 Is Critical for Actin Binding and Muscle Function in *Drosophila*. *International journal of molecular sciences*, *23*(5), 2533. https://doi.org/10.3390/ijms23052533
9. Malmqvist, U. P., Aronshtam, A., & Lowey, S. (2004). Cardiac myosin isoforms from different species have unique enzymatic and mechanical properties. *Biochemistry*, *43*(47), 15058–15065. https://doi.org/10.1021/bi0495329
10. Nag, S., Sommese, R. F., Ujfalusi, Z., Combs, A., Langer, S., Sutton, S., Leinwand, L. A., Geeves, M. A., Ruppel, K. M., & Spudich, J. A. (2015). Contractility parameters of human β-cardiac myosin with the hypertrophic cardiomyopathy mutation R403Q show loss of motor function. *Science Advances*, *1*(9), e1500511. https://doi.org/10.1126/sciadv.1500511
11. Karakikes, I., Ameen, M., Termglinchan, V., & Wu, J. C. (2015). Human induced pluripotent stem cell-derived cardiomyocytes: insights into molecular, cellular, and functional phenotypes. *Circulation research*, *117*(1), 80–88. https://doi.org/10.1161/CIRCRESAHA.117.305365

12. Ribeiro, A. J. S., Ang, Y.-S., Fu, J.-D., Rivas, R. N., Mohamed, T. M. A., Higgs, G. C., Srivastava, D., & Pruitt, B. L. (2015). Contractility of single cardiomyocytes differentiated from pluripotent stem cells depends on physiological shape and substrate stiffness. *Proceedings of the National Academy of Sciences of the United States of America*, *112*(41), 12705–12710. https://doi.org/10.1073/pnas.1508073112
13. Roberts, B., Hendershott, M. C., Arakaki, J., Gerbin, K. A., Malik, H., Nelson, A., Gehring, J., Hookway, C., Ludmann, S. A., Yang, R., Haupt, A., Grancharova, T., Valencia, V., Fuqua, M. A., Tucker, A., Rafelski, S. M., & Gunawardane, R. N. (2019). Fluorescent gene tagging of transcriptionally silent genes in hiPSCs. *Stem Cell Reports*, *12*(5), 1145–1158. https://doi.org/10.1016/j.stemcr.2019.03.001
14. Balafkan, N., Mostafavi, S., Schubert, M., Siller, R., Liang, K. X., Sullivan, G., & Bindoff, L. A. (2020). A method for differentiating human induced pluripotent stem cells toward functional cardiomyocytes in 96-well microplates. *Scientific Reports*, *10*(1), 18498. https://doi.org/10.1038/s41598-020-73656-2
15. Lian, X., Hsiao, C., Wilson, G., Zhu, K., Hazeltine, L. B., Azarin, S. M., Raval, K. K., Zhang, J., Kamp, T. J., & Palecek, S. P. (2012). Robust cardiomyocyte differentiation from human pluripotent stem cells via temporal modulation of canonical Wnt signaling. *Proceedings of the National Academy of Sciences of the United States of America*, *109*(27), E1848-57. https://doi.org/10.1073/pnas.1200250109
16. Lian, X., Bao, X., Al-Ahmad, A., Liu, J., Wu, Y., Dong, W., Dunn, K. K., Shusta, E. V., & Palecek, S. P. (2014). Efficient differentiation of human pluripotent stem cells to endothelial progenitors via small-molecule activation of WNT signaling. *Stem Cell Reports*, *3*(5), 804–816. https://doi.org/10.1016/j.stemcr.2014.09.005
17. Tohyama, S., Hattori, F., Sano, M., Hishiki, T., Nagahata, Y., Matsuura, T., Hashimoto, H., Suzuki, T., Yamashita, H., Satoh, Y., Egashira, T., Seki, T., Muraoka, N., Yamakawa, H., Ohgino, Y., Tanaka, T., Yoichi, M., Yuasa, S., Murata, M., … Fukuda, K. (2013). Distinct metabolic flow enables large-scale purification of mouse and human pluripotent stem cell-derived cardiomyocytes. *Cell Stem Cell*, *12*(1), 127–137. https://doi.org/10.1016/j.stem.2012.09.013
18. Pasqualin, C., Gannier, F., Yu, A., Malécot, C. O., Bredeloux, P., & Maupoil, V. (2016). SarcOptiM for ImageJ: high-frequency online sarcomere length computing on stimulated cardiomyocytes. *American Journal of Physiology. Cell Physiology*, *311*(2), C277-83. https://doi.org/10.1152/ajpcell.00094.2016
19. Lian, X., Zhang, J., Azarin, S. M., Zhu, K., Hazeltine, L. B., Bao, X., Hsiao, C., Kamp, T. J., & Palecek, S. P. (2013). Directed cardiomyocyte differentiation from human pluripotent stem cells by modulating Wnt/β-catenin signaling under fully defined conditions. *Nature Protocols*, *8*(1), 162–175. https://doi.org/10.1038/nprot.2012.150
20. Ahmed, R. E., Anzai, T., Chanthra, N., & Uosaki, H. (2020). A brief review of current maturation methods for human induced pluripotent stem cells-derived cardiomyocytes.

Frontiers in Cell and Developmental Biology, 8, 178. https://doi.org/10.3389/fcell.2020.00178
21. Walklate, J., Kao, K., Regnier, M., & Geeves, M. A. (2022). Exploring the super-relaxed state of myosin in myofibrils from fast-twitch, slow-twitch, and cardiac muscle. The Journal of Biological Chemistry, 298(3), 101640. https://doi.org/10.1016/j.jbc.2022.101640
22. Nag, S., & Trivedi, D. V. (2021). To lie or not to lie: Super-relaxing with myosins. *ELife*, *10*. https://doi.org/10.7554/eLife.63703
23. Alamo, L., Ware, J. S., Pinto, A., Gillilan, R. E., Seidman, J. G., Seidman, C. E., & Padrón, R. (2017). Effects of myosin variants on interacting-heads motif explain distinct hypertrophic and dilated cardiomyopathy phenotypes. eLife, 6, e24634. https://doi.org/10.7554/eLife.24634
24. de Tombe, P. P., & ter Keurs, H. E. D. J. (2016). Cardiac muscle mechanics: Sarcomere length matters. *Journal of Molecular and Cellular Cardiology*, *91*, 148–150. https://doi.org/10.1016/j.yjmcc.2015.12.006
25. Huethorst, E., Mortensen, P., Simitev, R. D., Gao, H., Pohjolainen, L., Talman, V., Ruskoaho, H., Burton, F. L., Gadegaard, N., & Smith, G. L. (2022). Conventional rigid 2D substrates cause complex contractile signals in monolayers of human induced pluripotent stem cell-derived cardiomyocytes. *The Journal of Physiology*, *600*(3), 483–507. https://doi.org/10.1113/JP282228
26. Moeller, J., Denisin, A. K., Sim, J. Y., Wilson, R. E., Ribeiro, A. J. S., & Pruitt, B. L. (2018). Controlling cell shape on hydrogels using lift-off protein patterning. *PloS One*, *13*(1), e0189901. https://doi.org/10.1371/journal.pone.0189901